coatings

MDPI

Article

Enhancing Thermoelectric Performance: The Impact of Carbon Incorporation in Spin-Coated Al-Doped ZnO Thin Films

Alberto Giribaldi [1,*], Cristiano Giordani [2,3], Giovanna Latronico [4], Cédric Bourgès [5,6], Takahiro Baba [7,8], Cecilia Piscino [1], Maya Marinova [9], Takao Mori [7,8], Cristina Artini [1,10], Hannes Rijckaert [11] and Paolo Mele [12,*]

1 Department of Chemistry and Industrial Chemistry, University of Genoa, Via Dodecaneso 31, 16146 Genoa, Italy; cecilia.piscino@edu.unige.it (C.P.); artini@chimica.unige.it (C.A.)
2 Institute of Physics, Faculty of Exact and Natural Sciences, Universidad de Antioquia—UdeA, Calle 70 No. 52-21, Medellín 050010, Colombia; cristiano.giordani@udea.edu.co
3 Grupo Productos Naturales Marinos, Faculty of Pharmaceutical and Food Sciences, Universidad de Antioquia—UdeA, Calle 70 No. 52-21, Medellín 050010, Colombia
4 National Research Council, Institute of Condensed Matter Chemistry and Technologies for Energy (CNR-ICMATE), Via G. Previati, 1/E, 23900 Lecco, Italy; giovannalatronico@cnr.it
5 International Center for Young Scientists (ICYS), National Institute for Materials Science (NIMS), 1-1 Namiki, Tsukuba 305-0044, Japan; cedric.bourges@unilim.fr
6 National Scientific Research Center, Institut de Recherche Sur Les Céramiques (CNRS-IRCER), UMR 7315, Centre Européen de la Céramique, 12 Rue Atlantis, 87068 Limoges, France
7 Research Center for Materials Nanoarchitectonics (MANA), National Institute for Materials Science (NIMS), 1-1 Namiki, Tsukuba 305-0044, Japan; baba.takahiro@nims.go.jp (T.B.); mori.takao@nims.go.jp (T.M.)
8 Graduate School of Pure and Applied Sciences, University of Tsukuba, 1-1-1 Tennoudai, Tsukuba 305-8577, Japan
9 National Scientific Research Center, National Agronomy Research Institute (CNRS-INRA), Centrale Lille, Université Artois, FR 2638—IMEC—Institut Michel-Eugène Chevreul, Université de Lille, 59000 Lille, France; maya.marinova@univ-lille.fr
10 National Research Council, Institute of Condensed Matter Chemistry and Technologies for Energy (CNR-ICMATE), Via De Marini 6, 16149 Genova, Italy
11 Department of Chemistry, Ghent University, Krijgslaan 281-S3, 9000 Ghent, Belgium; hannes.rijckaert@ugent.be
12 College of Engineering, Shibaura Institute of Technology, 307 Fukasaku, Minuma-ku, Saitama 337-8570, Japan
* Correspondence: s4839837@studenti.unige.it (A.G.); pmele@shibaura-it.ac.jp (P.M.)

Abstract: In the present study, for the first time, aluminum-doped zinc oxide (AZO) thin films with nanoinclusions of amorphous carbon have been synthesized via spin coating, and the thermoelectric performances were investigated varying the aging period of the solution, the procedure of carbon nanoparticles' addition, and the annealing atmosphere. The addition of nanoparticles has been pursued to introduce phonon scattering centers to reduce thermal conductivity. All the samples showed a strong orientation along the [002] crystallographic direction, even though the substrate is amorphous silica, with an intensity of the diffraction peaks reaching its maximum in samples annealed in the presence of hydrogen, and generally decreasing by the addition of carbon nanoparticles. Absolute values of the Seebeck coefficient improve when nanoparticles are added. At the same time, electric conductivity is higher for the sample with 1 wt.% of carbon and annealed in Ar with 1% of H_2, both increasing in absolute value with the temperature rise. Among all the samples, the lowest thermal conductivity value of 1.25 W/(m·K) was found at room temperature, and the highest power factor was 111 μW/(m·K^2) at 325 °C. Thus, the introduction of carbon effectively reduced thermal conductivity, while also increasing the power factor, giving promising results for the further development of AZO-based materials for thermoelectric applications.

Academic Editor: Carlos Jose Macedo Tavares

Received: 19 December 2024
Revised: 15 January 2025
Accepted: 16 January 2025
Published: 19 January 2025

Citation: Giribaldi, A.; Giordani, C.; Latronico, G.; Bourgès, C.; Baba, T.; Piscino, C.; Marinova, M.; Mori, T.; Artini, C.; Rijckaert, H.; et al. Enhancing Thermoelectric Performance: The Impact of Carbon Incorporation in Spin-Coated Al-Doped ZnO Thin Films. *Coatings* **2025**, *15*, 107. https://doi.org/10.3390/coatings15010107

Keywords: aluminum-doped zinc oxide; spin coating; carbon nanoparticles; thermoelectrics; thin films

1. Introduction

Thermoelectric devices for energy harvesting have attracted interest in recent years due to the need for more eco-friendly fuels to pursue the "energy transition" from fossil to renewable energy sources [1–5]. Thermoelectrics are not the final solution to this environmental issue, but they may constitute one of the many features of a new low-impact energetical landscape. Thermoelectric devices do not have moving parts and just rely on the thermoelectric properties of the materials they are made of, and on the temperature gradient they experience. To evaluate the performance of a thermoelectric material, and hence of a thermoelectric device, it is necessary to refer to the figure of merit ZT, introduced by Abraham F. Ioffe in his works on thermoelectricity [6–8]. As shown in Equation (1), this value depends on the Seebeck coefficient (S), the electric conductivity (σ), and the thermal conductivity (k), resulting from the sum of the electron (k_{el}) and the phonon (k_{ph}) contribution [8]:

$$ZT = \frac{\sigma \cdot S^2}{k_{el} + k_{ph}} \cdot T \quad (1)$$

Semiconductor materials, such as metal oxides for high-temperature applications [9], clathrates [10], skutterudites [11], half-Heusler intermetallics [12], some Zintl compounds [13], and chalcogenide compounds for low thermal conductivity and doping possibilities [14], are the most promising thermoelectric materials due to their potential various applications in this field [2,3,15].

Although most metal oxides usually show a low ZT due to their low σ and high k values, Al-doped zinc oxide (AZO) is among the compounds having moderate thermoelectric properties, which makes it suitable for high-temperature applications, i.e., in the temperature range where other thermoelectric materials with better performances are unstable. Moreover, AZO is nontoxic, cheap, and easy to synthesize, thus favoring its large-scale applications [16]. AZO has a ZnO hexagonal structure; namely, it is a semiconductor with a wide band gap of 3.4 eV and has proper doping with 2% of aluminum, which increases its electrical conductivity and therefore its power factor [17]. However, the high thermal conductivity remains an issue, keeping the ZT value low. Nanostructuring, dimensionality reduction, and the addition of nanoinclusions are approaches aimed at decreasing the value of k_{ph} [18,19], as all of them introduce scattering centers for phonons, which are responsible, along with conduction electrons, for thermal conductivity in crystalline solids. AZO thin films have already been investigated to determine the influence of the reduced dimensionality and the corresponding microstructure effect on its electrical properties. In particular, it has been found that the density of carriers and their scattering is mainly influenced by the presence of grain boundaries at the studied composition [20], and some interesting results are a resistance of 320 mΩ in a film with a thickness of 780 nm [21], a power factor of 550 mW/(m·K^2), and a thermal conductivity lower than 2 W/(m·K) [22,23], as well as a sheet resistance of 2.08 Ω/sq for a 1 µm thick film [24]. These promising results call for tuning of the thermoelectric performances of AZO through the control of morphology.

The subject of this work is the synthesis and the study of the thermoelectric properties of thin films of AZO with nanoinclusions of carbon with an average size of the primary particles being 12 nm, which can act as scattering centers for phonons reducing the value of k_{ph} without heavily affecting the other transport properties of the material. The carbon nanoparticles have been chosen because of their low price and use in large-scale applica-

tions. Since the approach consisting of the addition of nanoparticles to reduce the thermal conductivity has already been successfully applied to other systems, the thermoelectric performances of AZO thin films with nominal composition $Al_{0.02}Zn_{0.98}O$ are expected to be further enhanced. In particular, the figure of merit *ZT* of $In_{0.53}Ga_{0.47}As$ was increased by a factor of 2 with ErAs nanoparticles [25] and a thermal conductivity of 1 W/(m·K) in Si has been achieved with the introduction of Ge nanoparticles with a tailored size distribution [26]. Thin films were prepared by spin coating; the technique has been chosen for its operational simplicity and tunability of the different parameters, such as the aging period of the solution [27–31].

2. Materials and Methods

The solutions for the spin coating have been prepared dissolving $Zn(CH_3COO)_2{\cdot}2H_2O$ (Kanto Chemical Co., Inc., Tokyo, Japan, 99.0% min) and $AlCl_3{\cdot}6H_2O$ (Kanto Chemical Co., Inc., Tokyo, Japan, 98.0%) in 15 mL of isopropanol and 5 mL of ethanol in due amounts to obtain a solution of the precursor with a 98:2 ratio (0.15 mol/L for Zn and 0.003 mol/L for Al), corresponding to the chosen nominal composition. Then about 250 µL of 2-aminoethanol (Kanto Chemical Co., Inc., Tokyo, Japan, 99.0% min.) was added under stirring as a complexing agent, keeping the temperature at 60 °C until the volume of the solution was halved. The ratio between Al and Zn was the same for all the samples. An aging process, consisting of keeping the solution at room temperature for a certain time, as a step for a modified sol–gel method, was carried out on all the solutions, prior to the spin-coating process [24,27,28,30].

The series aged for different periods were prepared; they are referred to as "AZO 0 day" to "AZO 3 day", thus containing the information about the days of aging undergone by the spin-coating solution. Increasing the aging time results in an increasing opalescence and viscosity of the sol. Two drops of these solutions were deposited on a silica substrate (Crystal Base Co., Ltd., Osaka, Japan) of 10 mm × 10 mm with one smooth face, spun at 3000 rpm for 30 s with a K-35951 Kyowariken system, and fired at 350 °C for 10 min in a tubular furnace (TMF-500N, AS-ONE Co., Osaka, Japan) in ambient atmosphere. After repeating the process five times, films were annealed at 500 °C for 6 h under different atmospheres: low vacuum, O_2, Ar, and Ar + 1% of H_2. In Figure 1, the whole synthetic procedure is schematized. Amorphous carbon nanoparticles (BLACK PEARLS®2000, CABOT Co., Boston, MA, USA) were added in fractions of 0.5 wt.%, 1 wt.%, and 2 wt.% related to the quantity of the resulting AZO. The addition was performed before an aging process of 1 day in all the series and after the aging solely in the series annealed in Ar with 1% of H_2, using ultrasounds to homogenize the suspension. Samples added with carbon nanoparticles before and after aging are named "AZO-C" and "AZO-C after", respectively, with the name followed by the weight fraction of particles and the annealing atmosphere.

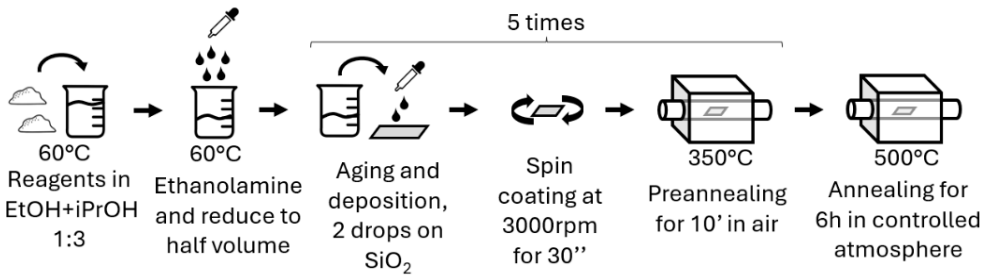

Figure 1. Synthesis protocol of the spin-coating film deposition of the samples.

Films were characterized through X-ray diffraction (XRD) by a SmartLab (Rigaku Co., Tokyo, Japan) using the wavelength Kα of Cu (voltage 40 kV, current 50 mA) in the range

10–100° with a step of 0.02°, a speed of 2°/min, and a slit of 5 mm. The SEM imaging was made with a JSM-7100F (JEOL Ltd., Tokyo, Japan) Field Emission Scanning Electron Microscope using the secondary electrons signal and an operating voltage of 10 kV. The thicknesses of the films were determined with an MI4050 Focused Ion Beam System (FIB) (Hitachi, Tokyo, Japan) to etch the sample and then measure it via imaging mode. The microstructure of the AZO thin films was analyzed by transmission electron microscopy (TEM). For TEM investigations, a cross-sectional lamella was prepared by FIB, employing an FEI Nova 600 Dual Beam system (Nanolab, Waltham, MA, USA), based on the procedure described in this technical note [32]. The experiment was performed on the TITAN Themis at 300 kV in Scanning TEM (STEM) mode with high-angle annular dark-field (HAADF) and energy-dispersive X-ray spectroscopy (EDX). The STEM has been performed using a semi-convergence of 20 mrad and a spot size of 0.5 nm. Preliminary room temperature values of the Seebeck coefficient and sheet resistance (R_S) have been pursued via a Portable Thermoelectric Meter–3 (JouleYacht, Wuhan, China) and a Loresta-FX MCP-T380 (NH Instruments, Willich, Germany) using the RMH504 four-point probe (NH Instruments, Willich, Germany). S and σ were simultaneously measured by the four-probe method using a ZEM-3 (ULVAC Advance-Riko, Yokohama, Japan) device in temperature under partial helium pressure, from 25 °C to 325 °C with a step of 50 °C. The cross-plane thermal conductivity (k_{cp}) has been determined by a picosecond thermoreflectance method using a front-heating front-detection setup [33].

3. Results and Discussion

The XRD patterns of all the samples exhibit a peak at 2θ = 34.4° corresponding to the [002] crystallographic direction of the $P6_3mc$ ZnO wurtzite phase; just one other peak appears at 2θ~73.6° related to the [004] direction. This evidence denotes a strongly oriented growth of the diffraction domains of thin films, even if the deposition has been carried on amorphous silica, also observed when depositing thin films of the same material by pulsed laser deposition (PLD) [22,34,35]. The intensity of the [002] peak decreases with the addition of carbon nanoparticles, and it depends on the annealing atmosphere, being the highest for samples treated in Ar + 1%H_2, followed by samples treated in Ar (Figure 2). This result is in accordance with the observation of another study, that stated the suitability of an annealing in the presence of H_2 with respect to one with air for AZO [36]. An intensity decrease (Figure 3) and a peak area decrease (Figure 4) were observed when nanoparticles were added to the spin-coating solution after the aging period. Using the relation between d_{hkl} and lattice parameters in a hexagonal structure, the value of c was determined to be 0.5080(2) nm for all the samples with the exception of the ones with nanoparticles annealed in Ar + 1% H_2, which show a slightly higher c value of 0.5085 nm. This value is significantly lower than the one found in the literature for both ZnO and Fe-doped ZnO (c of 0.5205 nm for the former and c of 0.5202 nm for the latter with 10% Fe) [37] and from the JCPDS 89-7102, as a consequence of the presence of the smaller Al instead of Zn.

The microstructure observed by SEM of the films without carbon consists of a homogeneous texture with surface ripples (Figure 5a,b), which seem to be reduced by longer aging. The addition of carbon nanoparticles completely removes these deformations and leaves a wave-like pattern of more rough regions with a radial distribution from the center of the substrate, visible at lower magnification (Figure 5c). This is probably due to the deposition method, which involves the spinning of the substrate around the normal axis through its center. A peculiar morphology is present solely in the sample annealed in the presence of hydrogen: some grains of the order of 100 nm seem to stand out from the surface of the plain regions as well as of the rough ones (Figure 5d). These samples are also the only ones whose color remains dark and resembles the respective spin-coating

solutions after the thermal treatment, suggesting the preservation of the nanoparticles after the thermal treatment.

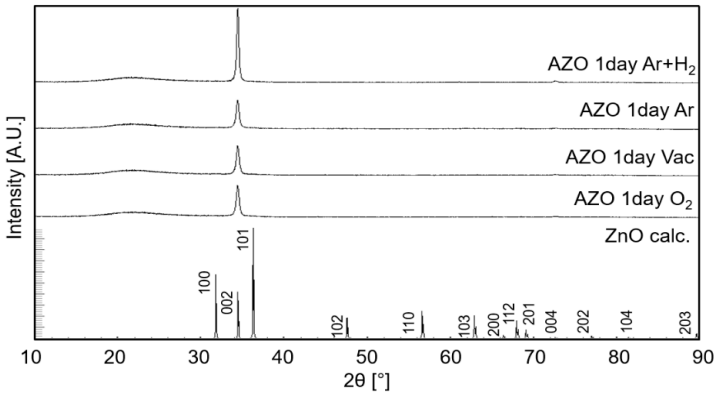

Figure 2. XRD patterns of samples without carbon nanoparticles and annealed under different atmospheres, namely, Ar + H_2, Ar, O_2, and vacuum. The calculated pattern for the wurtzite type ZnO phase is shown as a reference [37]. The broad peak between 15° and 25° is due to the amorphous phase of the silica substrate.

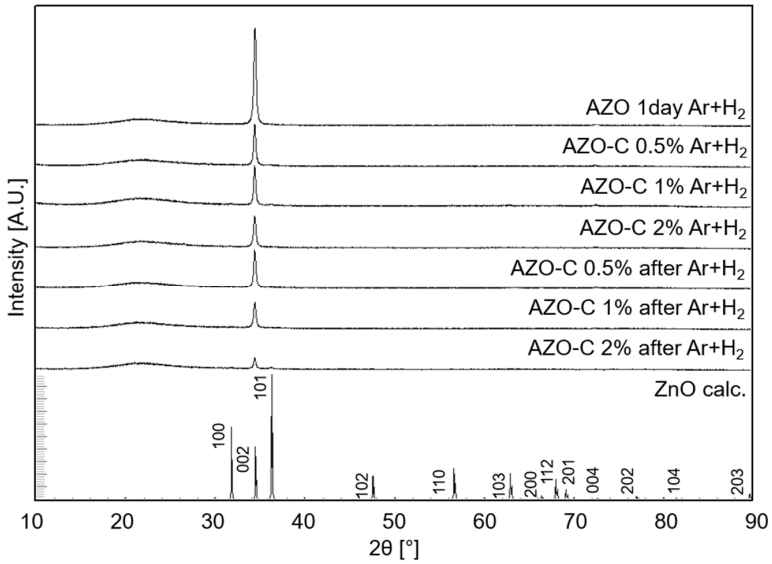

Figure 3. XRD patterns of all the samples annealed in Ar + H_2.

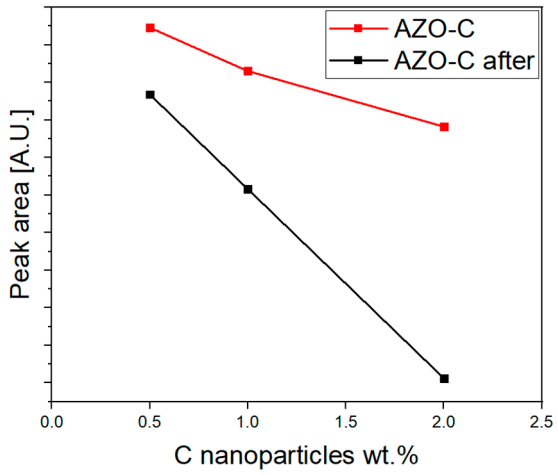

Figure 4. Areas of the [002] diffraction peaks in the series with the addition of nanoparticles before the aging (AZO-C) and the series with the addition afterward (AZO-C after).

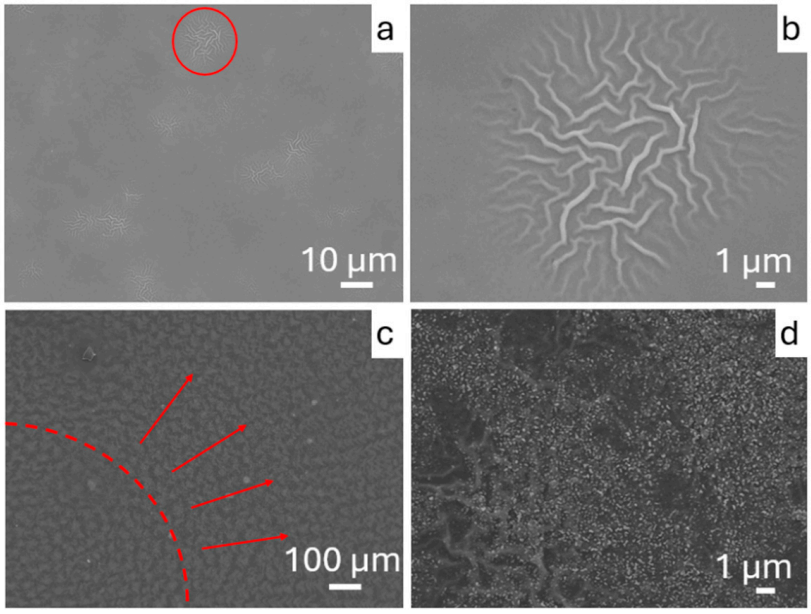

Figure 5. SEM secondary electrons images of (**a**) AZO 1 day; (**b**) detail of the highlight in (**a**); (**c**) AZO-C 0.5% Ar + H_2 with the limit of the center of the film and the direction of the wave-like pattern marked; (**d**) detail of (**c**).

The observed thickness of the films from the cross-sectional HAADF images acquired with the STEM is 161 ± 3 nm for "AZO 1 day Ar + H_2" and 123 ± 3 nm for "AZO-C 1% Ar + H_2". The single-layer thickness is, on average, higher in "AZO 1 day" and has a lower variability than in "AZO-C 1% Ar + H_2". Moreover, in "AZO-C 1% Ar + H_2", the thickness decreases from the first to the last layer in order of deposition; the grains are generally smaller and their packing is less dense than in "AZO 1 day Ar + H_2". Amorphous regions, which may be in part the carbon nanoparticles, since some of them show dimensions and shapes coherent with the nanoparticles employed, are found in this sample (Figure 6). The resulting morphology, with more abrupt discontinuities, such as grain boundaries, discontinuous interfaces, and amorphous portions of materials, can explain the further suppression of the thermal conductivity observed in "AZO-C 1% Ar + H_2". The presence of aggregates or nanoparticles of C, however, is not fully confirmed.

The results of the measurements of room temperature S and R_S have been used as screening tests to determine the most promising samples in terms of thermoelectric performance. All the samples show negative S, with AZO being an n-type semiconductor, so the discussion below is based on the module of this quantity. The trends of S and R_S are very similar through the same series. The aging period does not heavily influence the value of S for up to two days, keeping a stable value of about −180 µV/K at room temperature for the first three samples of the series (from AZO 0 day Ar + H_2 to AZO 2 day Ar + H_2). On the contrary, when the aging reaches three days (AZO 3 day Ar + H_2), S and R_S abruptly decrease (Figure 7). These films have a rather low R_S at room temperature, in the order of the tens of kΩ/sq. Overall, taking into account the XRD patterns, the thermoelectric features, and the complexity of the method, the best choice seems to be 1-day aging. Therefore, the following discussions refer to samples synthesized from a solution aged for 1 day.

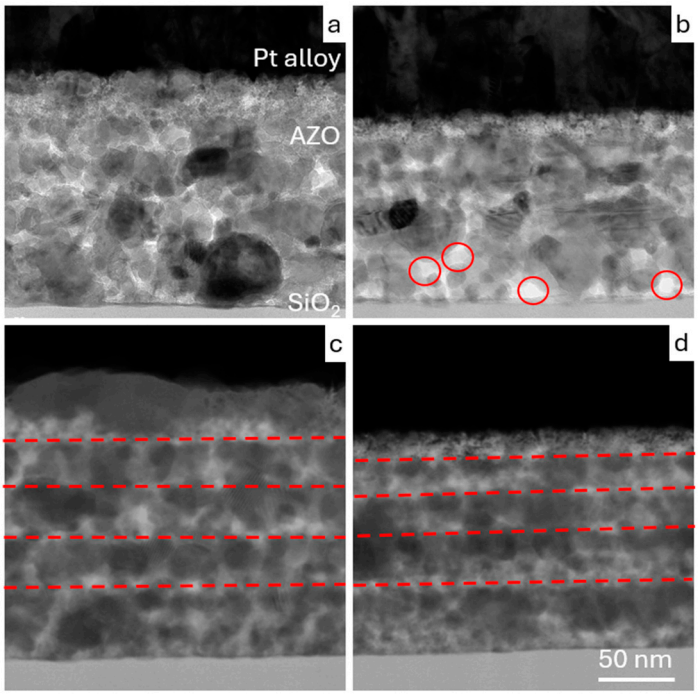

Figure 6. Cross-sectional TEM images of (**a**) AZO 1 day Ar + H_2 and (**b**) AZO-C 1% Ar + H_2, highlighting the amorphous areas more likely to be carbon nanoparticles; and HAADF-STEM images of (**c**) AZO 1 day Ar + H_2 and (**d**) AZO-C 1% Ar + H_2, with the layer structure highlighted.

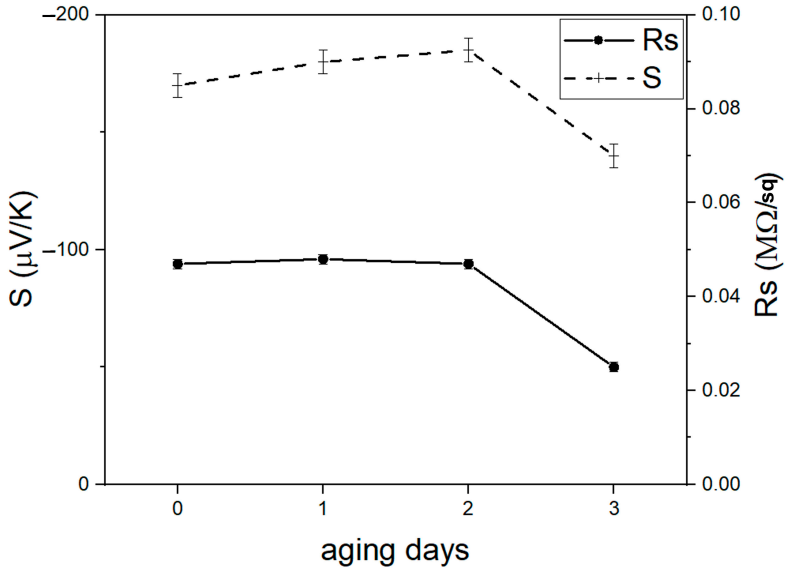

Figure 7. Preliminary room temperature values of S and R_S of the samples AZO without carbon and annealed in Ar + H_2, showing the dependence on the aging period of the solution.

The addition of carbon nanoparticles, carried out to reduce thermal conductivity by the introduction of scattering centers, has a different influence on the room temperature values of S and R_S depending on the atmospheric conditions adopted for the annealing process, as depicted in Figure 8. In samples "AZO-C" annealed in Ar and Ar + H_2, an overall reduction in S and R_S can be observed with increasing the fraction of carbon nanoparticles. The trend is inverted in the samples "AZO-C after" annealed in Ar + H_2, while no clear dependence appears in samples annealed in O_2 and vacuum, whose higher sheet resistance and higher Seebeck coefficient are a direct consequence of the far lower conductivity. The samples annealed in Ar + H_2 are the only two series that seem to preserve the carbon nanoparticles after the thermal treatment, thanks to the mild reducing conditions. Out of these samples,

the ones synthesized with the carbon introduced before aging also show a R_S lower by an order of magnitude with respect to the others. The other annealing atmospheres, namely, Ar (blue curve), O_2 (green curve), and vacuum (yellow curve), cause an abrupt increase in R_S and consequently in S at room temperature compared to the ones annealed in Ar + H_2 (red curve), as shown in Figure 8. In particular, S ranges from −200 µV/K to −650 µV/K in these samples against the values between −100 µV/K and −200 µV/K of "AZO-C Ar + H_2", while R_S increases by almost two orders of magnitude, from around 0.04 MΩ/sq to values ranging from 0.2 MΩ/sq to 1.5 MΩ/sq. Therefore, the best compromise between S and R_S stands in the samples annealed in Ar + H_2 with the carbon nanoparticles added before the aging of 1 day.

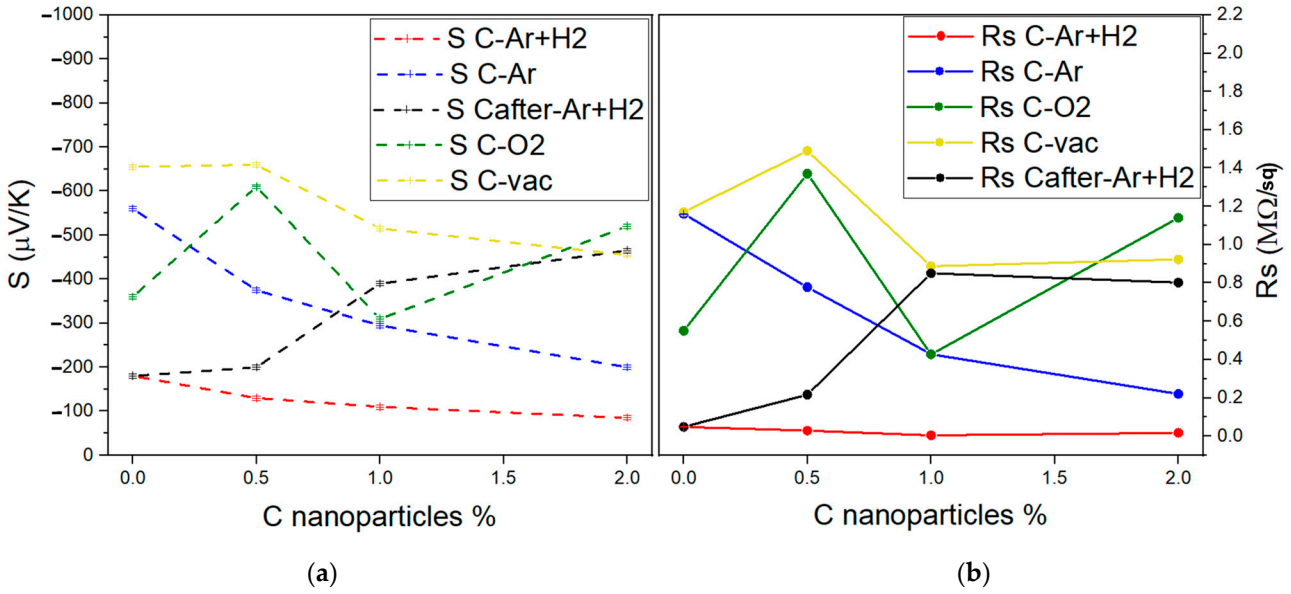

(**a**) (**b**)

Figure 8. Preliminary room temperature values of S (**a**) and R_S (**b**) of samples AZO, as a function of C addition in the 1-day aging samples, annealed at 500 °C in various atmospheres.

From the room temperature thermoelectric performances and the considerations about the retention of the nanoparticles, the samples that show the best trade-off between low resistance and high Seebeck coefficient, while seemingly preserving the carbon nanoparticles, are the samples "AZO-C Ar + H_2". Out of these, "AZO-C 1% Ar + H_2" has been chosen as a representative sample of the series. Therefore, "AZO-C 1% Ar + H_2" has been measured, along with "AZO 1 day Ar + H_2" as a reference without carbon, with the ZEM-3 system under partial helium pressure and σ was calculated using the thickness obtained via TEM observations. Both S and σ increase with temperature and show a hysteresis between heating and cooling, as evident from the data depicted in Figure 9. These show anomalous behavior with abrupt modifications of their properties when heated for the first time, without changes in the appearance of the thin film, probably because the measurement itself acted as an annealing, as observed in other studies [38,39]. S seems to increase when the nanoparticles are added, in contrast with what was observed at room temperature, even though the values are comparable between the samples with different fractions of C. Instead, no meaningful conclusions can be drawn for the dependence of σ, which is higher for "AZO-C 1% Ar + H_2" even in comparison with "AZO 1 day Ar + H_2". The power factor reaches its maximum of about 111 µW/(m·K^2) at 325 °C in "AZO-C 1% Ar + H_2" (Figure 9c), which also shows the lowest value of k. The values of k at room temperature of the thin films have been calculated from the thermoreflectance data and assuming the heat capacity and density of AZO being 480 J/(kg·K) and 5.195 g/cm^3, respectively. The sample

"AZO 1 day Ar + H_2" shows a k_{cp} of 2.55 ± 0.28 W/(m·K), against 1.25 ± 0.15 W/(m·K) of "AZO-C 1% Ar + H_2". This means that the carbon addition caused a lowering of k, although the details of the mechanism that causes this suppression and the presence of carbon are yet to be confirmed. Furthermore, these values are both significantly lower than 10 W/(m·K), the value typically encountered in films of the same material obtained by pulsed laser deposition [40], suggesting the influence of the deposition method. In particular, the layer-based morphology resulting from the spin-coating method introduces interfaces and discontinuities that act as scattering centers for phonons, at least for the cross-plane direction of the thin film.

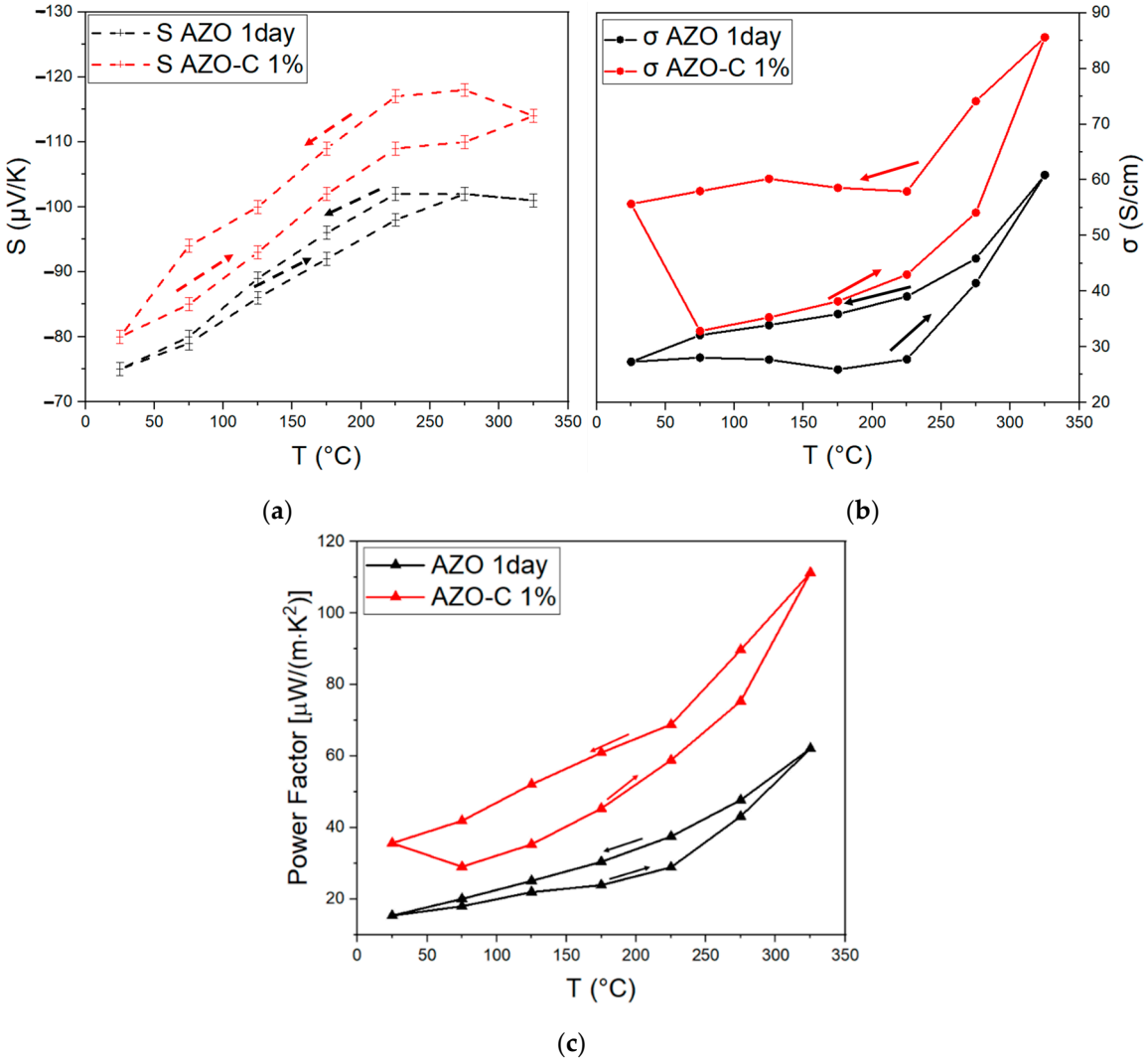

Figure 9. S (**a**) and σ (**b**) of samples "AZO 1 day Ar + H_2" and "AZO-C Ar + H_2", as a function of temperature during heating and cooling; (**c**) calculated power factor of the samples "AZO 1 day Ar + H_2" and AZO-C 1% Ar + H_2" showing the dependence with respect to the temperature during heating and cooling.

4. Conclusions

The [00l] oriented AZO thin film samples, synthesized via spin coating, showed enhanced thermoelectric performance, thanks to both the chemical deposition method and the introduction of nanoparticles. The lowest thermal conductivity value was 1.25 W/(m·K) at room temperature, and the highest power factor was 111 μW/(m·K^2) at 325 °C. The crystallinity degree increases with the aging period of the spin-coating solution and decreases if the carbon nanoparticles are added. The amorphous carbon nanoparticles, which seem

to be retained only after annealing in Ar + H_2, cause inhomogeneity in the morphology of the thin films and do not heavily influence the values of the Seebeck coefficient, though electrical conductivity slightly increases, and the cross-plane thermal conductivity is efficiently suppressed. In this respect, carbon seems to induce a slight strain in the lattice, as suggested by the values of the c-axis, and mass fluctuations without dampening the electrical conductivity, giving better results when the addition is performed before the aging process. Further studies on spin-coated AZO thin films are to be pursued, for instance, to evaluate the layers' thickness dependence from the synthetic protocol and its drawbacks on the thermoelectric properties, and to optimize the method. Moreover, further investigation about the retention (through Raman Spectroscopy or Induction-Coupled Plasma Optical Emission Spectroscopy, for instance) and the exact role of the carbon nanoparticles in the k_{cp} suppression are necessary to better apply this solution to this and other thermoelectric materials.

Author Contributions: Conceptualization, A.G., P.M. and G.L.; methodology, A.G., P.M., C.G., H.R., M.M. and G.L.; formal analysis, P.M. and A.G.; investigation, A.G., P.M., G.L., C.B., T.B., M.M. and C.G.; resources, P.M., C.A. and T.M.; data curation, A.G.; writing—original draft preparation, A.G.; writing—review and editing, P.M., A.G., G.L, C.G., C.B., T.B., C.A., T.M., H.R., C.P. and M.M.; visualization, A.G.; supervision, P.M. and C.A.; project administration, P.M.; funding acquisition, T.M. All authors have read and agreed to the published version of the manuscript.

Funding: H.R. acknowledges support and funding as a postdoctoral fellow in fundamental research of the Research Foundation—Flanders (FWO) under grant number 1273621N. T.M. and T.B. are thankful for the support from JST Mirai JPMJMI19A1.

Institutional Review Board Statement: Not applicable.

Informed Consent Statement: Not applicable.

Data Availability Statement: The data presented in this research study are available in this article.

Acknowledgments: P.M. and C.G. are thankful to the Shibaura Institute of Technology (Japan) and Universidad de Antioquia (Colombia) for their cooperation framework agreement and support for the project n. 2022-48030 titled: "Development of oxide thin films embedded with polymer nanoparticles for the realization of environmentally friendly thermoelectric harvesters". P.M, A.G., and G.L. are grateful to Alicja Klimkowicz (Shibaura Institute of Technology, Japan) for the assistance in the microscopical observations of nanoparticles. P.M. and C.G. are also grateful to Antonino Tamburello (UER, Rome, Italy) for insightful inspiration.

Conflicts of Interest: The authors declare no conflicts of interest.

References

1. Riffat, S.B.; Ma, X. Thermoelectrics: A review of present and potential applications. *Appl. Therm. Eng.* **2003**, *23*, 913–935. [CrossRef]
2. Sootsman, J.R.; Chung, D.Y.; Kanatzidis, M.G. New and old Concepts in Thermoelectric Materials. *Angew. Chem.* **2009**, *48*, 8616–8639. [CrossRef] [PubMed]
3. He, J.; Tritt, T.M. Advances in Thermoelectric Materials Research: Looking Back and Moving Forward. *Science* **2017**, *357*, 1369. [CrossRef] [PubMed]
4. Russ, B.; Glaudell, A.; Urban, J.; Chabinyc, M.L.; Segalman, R.A. Organic thermoelectric materials for energy harvesting and temperature control. *Nat. Rev. Mater.* **2016**, *1*, 16050. [CrossRef]
5. D'Angelo, M.; Galassi, C.; Lecis, N. Thermoelectric Materials and Applications: A Review. *Energies* **2023**, *16*, 6409. [CrossRef]
6. Ioffe, A.F. *Semiconductor Thermoelements and Thermoelectric Cooling*; Infosearch Ltd.: London, UK, 1957.
7. Ioffe, A.F. The Revival of Thermoelectricity. *Sci. Am.* **1958**, *199*, 31–37.
8. Vedernikov, M.V.; Iordanishvili, E.K. AF Ioffe and Origin of Modern Semiconductor Thermoelectric Energy Conversion. In Proceedings of the Seventeenth International Conference on Thermoelectrics. Proceedings ICT98 (Cat. No. 98TH8365), Nagoya, Japan, 28–28 May 1998; pp. 37–42.

9. Walia, S.; Balendhran, S.; Nili, H.; Zhuiykov, S.; Rosengarten, G.; Wang, Q.H.; Bhaskaran, M.; Sriram, S.; Strano, M.S.; Kalantar-zadeh, K. Transition metal oxides—Thermoelectric properties. *Progr. Mater. Sci.* **2013**, *58*, 1443–1489. [CrossRef]
10. Dolyniuk, J.-A.; Owens-Baird, B.; Wang, J.; Zaikina, J.V.; Kovnir, K. Clathrate thermoelectrics. *Mater. Sci. Eng. R Rep.* **2016**, *108*, 1–46. [CrossRef]
11. Zhao, C.; Wang, M.; Liu, Z. Research progress on preparation methods of skutterudite. *Inorganics* **2022**, *10*, 106. [CrossRef]
12. Aversano, F.; Palumbo, M.; Ferrario, A.; Boldrini, S.; Fanciulli, C.; Baricco, M.; Castellero, A. Role of secondary phases and thermal cycling on thermoelectric properties of TiNiSn half-Heusler alloy prepared by different processing routes. *Intermetallics* **2020**, *127*, 106988. [CrossRef]
13. Bano, S.; Chetty, R.; Jayachandran, B.; Mori, T. $Mg_3(Sb,Bi)_2$-based materials and devices rivalling bismuth telluride for thermoelectric power generation and cooling. *Device* **2024**, *2*, 100408. [CrossRef]
14. Wang, Y.; Lin, P.; Lou, Q.; Zhang, Z.; Huang, S.; Lu, Y.; He, J. Design guidelines for chalcogenide-based flexible thermoelectric materials. *Mater. Adv.* **2021**, *2*, 2584–2593. [CrossRef]
15. Artini, C.; Pennelli, G.; Graziosi, P.; Li, Z.; Neophytou, N.; Melis, C.; Colombo, L.; Isotta, E.; Lohani, K.; Scardi, P.; et al. Roadmap on Thermoelectricity. *Nanotechnology* **2023**, *34*, 292001. [CrossRef] [PubMed]
16. Wang, Y.; Zhou, C.; Elquist, A.M.; Ghods, A.; Saravade, V.G.; Lu, N.; Ferguson, I. A review of earth abundant ZnO-based materials for thermoelectric and photovoltaic applications. In Proceedings of the Proceedings Volume 10533, Oxide-based Materials and Devices IX, San Francisco, CA, USA, 27 January–1 February 2018; p. 105331R.
17. Zhou, B.; Chen, L.; Li, C.; Qi, N.; Chen, Z.; Su, X.; Thang, X.F. Significant Enhancement in the Thermoelectric Performance of Aluminum-doped ZnO Tuned by Pore Structure. *ACS Appl. Mater. Interfaces* **2020**, *12*, 51669–51678. [CrossRef]
18. Vineis, C.J.; Shakouri, A.; Majumdar, A.; Kanatzidis, M.G. Nanostructured Thermoelectrics: Big Efficiency Gains from Small Features. *Adv. Mater.* **2010**, *22*, 3970–3980. [CrossRef]
19. Noori, A.; Masoumi, S.; Hashemi, N. Temperature Dependence of the Seebeck Coefficient in Zinc Oxide Thin Films. *J. Phys. Conf. Ser.* **2017**, *939*, 012013. [CrossRef]
20. Jia, J.; Oka, N.; Kusayanagi, M.; Nakatomi, S.; Shigesato, Y. Origin of Carrier Scattering in Polycrystalline Al-doped ZnO Films. *Appl. Phys. Express* **2014**, *7*, 105802. [CrossRef]
21. Zhou, H.M.; Yi, D.; Yu, Z.; Xiao, L.; Li, J. Preparation of Aluminum Doped Zinc Oxide Films and the Study of their Microstructure, Electrical and Optical Properties. *Thin Solid. Films* **2007**, *15*, 6909–6914. [CrossRef]
22. Mele, P.; Saini, S.; Honda, H.; Matsumoto, K.; Miyazaki, K. Effect on Substrate on Thermoelectric Properties of Al-doped ZnO Thin Films. *Appl. Phys. Lett.* **2013**, *102*, 253903. [CrossRef]
23. Nam, W.H.; Lim, Y.S.; Choi, S.M.; Seo, W.S.; Lee, J.Y. High-Temperature Charge Transport and Thermoelectric Properties of a Degenerately Al-doped ZnO Nanocomposite. *J. Mater. Chem.* **2012**, *22*, 14633–14638. [CrossRef]
24. Tonny, K.N.; Rafique, R.; Sharmin, A.; Bashar, M.S.; Mahmood, Z.H. Electrical, Optical and Structural Properties of Transparent Conducting Al doped ZnO (AZO) Deposited by Sol-Gel Spin Coating. *AIP Adv.* **2018**, *8*, 065307. [CrossRef]
25. Kim, W.; Zide, J.; Gossard, A.; Klenov, D.; Stemmer, S.; Shakouri, A.; Majumdar, A. Thermal Conductivity Reduction and Thermoelectric Figure of Merit Increase by Embedding Nanoparticles in Crystalline Semiconductors. *PRL* **2006**, *96*, 045901. [CrossRef] [PubMed]
26. Zhang, H.; Minnich, A.J. The Best Nanoparticle Size Distribution for Minimum Thermal Conductivity. *Sci. Rep.* **2015**, *5*, 8995. [CrossRef] [PubMed]
27. Wang, Y.; Xu, G.; Yang, J.; Mao, W.; Wang, J.; Liu, Z.; Dong, Y.; Yang, S.; Li, J. Fabrication of AZO and FAZO Films Using Low-cost Spin-Coating Method. *Opt. Mater.* **2022**, *126*, 112204. [CrossRef]
28. Lee, W.; Leem, J.Y. Enhancement of the Ultraviolet Photoresponsivity of Al-doped ZnO Thin Films Prepared by using the Sol-gel Spin-coating Method. *J. Korean Phys. Soc.* **2018**, *72*, 610–614. [CrossRef]
29. Nga, Z.N.; Chana, K.Y.; Tohsophonb, T. Effects of Annealing Temperature on ZnO and AZO Films Prepared by Sol–Gel Technique. *Appl. Surf. Sci.* **2012**, *258*, 9604–9609. [CrossRef]
30. Kumar, K.D.A.; Valanarasu, S.; Kathalingam, A.; Ganesh, V.; Shkir, M.; AlFaify, S. Effect of solvents on sol–gel spin-coated nanostructured Al-doped ZnO thin films: A film for key optoelectronic applications. *Appl. Phys. A* **2017**, *123*, 801. [CrossRef]
31. Sengupta, J.; Sahoo, R.K.; Mukherjee, C.D. Effect of annealing on the structural, topographical and optical properties of sol–gel derived ZnO and AZO thin films. *Mater. Lett.* **2012**, *83*, 84–87. [CrossRef]
32. Rijckaert, H. Preparation of the S/TEM Lamella of Commercial $REBa_2Cu_3O_{7-x}$ Coated Conductors by FIB. *IEEE Trans. Appl. Supercond.* **2024**, *34*, 7500707. [CrossRef]
33. Baba, T.; Baba, T.; Mori, T. Fourier Transform Thermoreflectance method Under Front-Heat Front-Detect Configuration. *Int. J. Thermophys.* **2021**, *45*, 61. [CrossRef]
34. Chen, X.; Guan, W.; Fang, G.; Zhao, X.Z. Influence of substrate temperature and port-treatment on the properties of AnO:Al thin films prepared by pulsed laser deposition. *Appl. Surf. Sci.* **2005**, *252*, 1561–1567. [CrossRef]

35. Alyamani, A.; Sayari, A.; Albadri, A.; Albrithen, H.; El Mir, L. Structural, morphological and optical characterizations of ZnO:Al thin films grown on silicon substrates by pulsed laser deposition. *Eur. Phys. J. Plus* **2016**, *131*, 328. [CrossRef]
36. Wang, W.P.; Chen, Y.Y.; Hsu, J.C.; Wang, C. Structural, optical and electrical properties of aluminum doped ZnO films annealed in air and hydrogen atmosphere. *J. Non-Cryst. Solids* **2014**, *383*, 131–136. [CrossRef]
37. Saadi, H.; Rhouma, F.I.H.; Benzarti, Z.; Bougrioua, Z.; Guemazi, S.; Khirouni, K. Electrical Conductivity Improvement of Fe doped ZnO Nanopowders. *Mater. Res. Bull.* **2020**, *129*, 110884. [CrossRef]
38. Abdullin, K.A.; Gabdullin, M.T.; Zhumagulov, S.K.; Ismailova, G.A.; Gritsenko, L.V.; Kedruk, Y.Y.; Mirzaeian, M. Stabilization of the Surface of ZnO Films and Elimination of the Aging Effect. *Materials* **2021**, *14*, 6535. [CrossRef]
39. Zhang, W.; Chen, X.; Ma, Y.; Xu, Z.; Wu, L.; Yang, Y.; Tsang, S.W.; Chen, S. The Positive Aging Effect of ZnO Nanoparticles Induced by Surface Stabilization. *J. Phys. Chem. Lett.* **2020**, *11*, 5863–5870. [CrossRef]
40. Darwish, A.M.; Muhammad, A.; Sarkisov, S.S.; Mele, P.; Saini, S.; Liu, J.; Shiomi, J. Thermoelectric Properties of Al-doped ZnO Composite Films with Polymer Nanoparticles Prepared by Pulsed Laser Deposition. *Composites Part. B* **2019**, *167*, 406–410. [CrossRef]